ACS OMEGA

http://pubs.acs.org/journal/acsodf

Article

# Selective Chemistry-Based Separation of Semiconducting Single-Walled Carbon Nanotubes and Alignment of the Nanotube Array Network under Electric Field for Field-Effect Transistor Applications

Thomaati Haridass Vignesh Kumar, Jerome Rajendran, Ramila D. Nagarajan, Gayathri Jeevanandam, Anatoly N. Reshetilov, and Ashok K. Sundramoorthy*

Cite This: *ACS Omega* 2021, 6, 5146−5157

Read Online

ACCESS | Metrics & More | Article Recommendations | Supporting Information

**ABSTRACT:** Semiconducting single-walled carbon nanotubes (s-SWCNTs) are considered as a replacement for silicon in field-effect transistors (FETs), solar cells, logic circuits, and so forth, because of their outstanding electronic, optical, and mechanical properties. Herein, we have studied the reaction of pristine SWCNTs dispersed in a pluronic F-68 (PF-68) polymer solution with para-amino diphenylamine diazonium sulfate (PADDS) to separate nanotubes based on their metallicity. The preferential selectivity of the reactions was monitored by changes in the semiconducting ($S_{22}$ and $S_{33}$) and metallic ($M_{11}$) bands by ultraviolet−visible−near infrared spectroscopy. Metallic selectivity depended on the concentrations of PADDS, reaction time, and the solution pH. Furthermore, separation of pure s-SWCNTs was confirmed by Raman spectroscopy and Fourier-transform infrared spectroscopy. After the removal of metallic SWCNTs, direct current electric field was applied to the pure s-SWCNT solution, which effectively directed the nanotubes to align in one direction as nanotube arrays with a longer length and high density. After that, electrically aligned s-SWCNT solution was cast on a silicon substrate, and the length of the nanotube arrays was measured as ∼2 to ∼14 $\mu$m with an areal density of ∼2 to ∼20 tubes/$\mu$m of s-SWCNTs. Next, electrically aligned s-SWCNT arrays were deposited on the channel of the FET device by drop-casting. Field-emission scanning electron microscopy and electrical measurements have been carried out to test the performance of the aligned s-SWCNTs/FETs. The fabricated FETs with a channel length of 10 $\mu$m showed stable electrical properties with a field-effect mobility of 30.4 $cm^2$/Vs and a $\log_{10}$ ($I_{on}/I_{off}$) current ratio of 3.96. We envisage that this new chemical-based separation method and electric field-assisted alignment could be useful to obtain a high-purity and aligned s-SWCNT array network for the fabrication of high-performance FETs to use in digital and analog electronics.

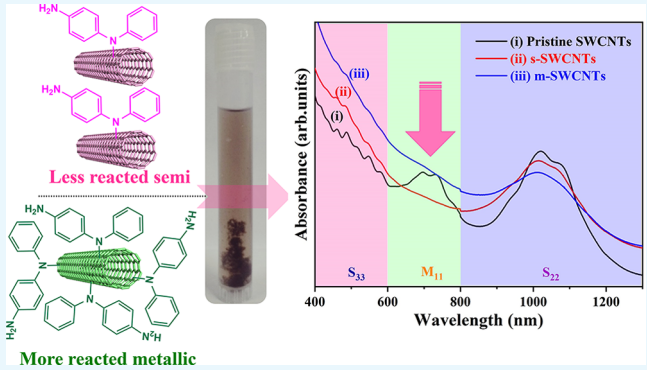


## 1. INTRODUCTION

Semiconducting single-walled carbon nanotubes (s-SWCNTs) with a tunable bandgap (0.5 to 0.8 eV)[1] and high field-effect mobility (79,000 $cm^2$/Vs)[1] showed great promise in digital electronics,[2] field-effect transistors (FETs),[3] radiofrequency circuits,[4] integrated circuits,[5] radiation hard memory,[6] infrared-based detectors,[7] and sensors with flexible and stretchable electronics.[8,9] For instance, s-SWCNTs could deliver ten times higher energy-efficiency than conventional metal oxide based-semiconductor FETs because of their ballistic electron transport, excellent mechanical properties, strong optical absorptivity, very large Seebeck coefficient (160 $\mu$V/K), near-infrared absorption (900−1400 nm), and optimal electrostatics.[10] In particular, high-purity s-SWCNTs have gained more interest in the development of low-power, transparent, and high-performance display techniques for Internet of Things, smart phones, television, computers, and so forth.[1]

Generally, all known synthetic methods could produce SWCNTs with various heterogeneities in terms of metallicity, diameter, length, and chirality, which significantly affect the high-end applications of SWCNTs. Even, the presence of a trace amount of metallic SWCNTs (m-SWCNTs) could degrade the on/off ratio of the devices because of short circuit of the source and drain electrodes in transistors.[11] The mass production of high-purity s-SWCNTs is still required, and it remains challenging because of several factors.[1−3,10] To separate s-SWCNTs from a pristine SWCNT mixture, several methods

Received: September 19, 2020
Accepted: February 5, 2021
Published: February 16, 2021

**Scheme 1. (a) 2-D Structural Formula of PF-68 (Red Regions Represent Hydrophilic Nature, while Green Regions Are Hydrophobic), (b) Various Steps Involved in the Preparation of Monodispersed SWCNTs in PF-68 Aqueous Solution, and (c) Proposed Interaction between PF-68 and SWCNTs in Aqueous Solution**

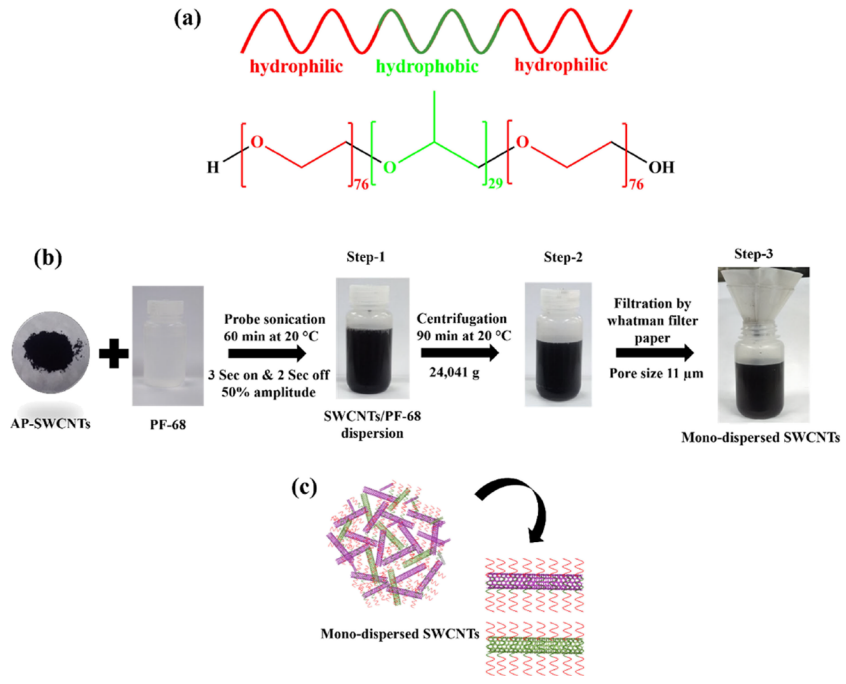


have been developed such as density gradient ultracentrifugation (DGU),[12] gel chromatography,[11] electrophoresis,[13,14] aqueous two-phase extraction,[15] charge sign reversal method,[16] DNA wrapping,[17] and so on. However, after the separation of s-SWCNTs, if the purity is low, it can cause serious problems in the function of transistors.[18,19] Using DGU, separation of s-SWCNTs could be achieved in low quantity (~0.00035 mmol/day) but with high purity.[20] Gel chromatography might have produced a high yield of semiconducting SWCNTs (~0.02704 mmol/day), but the purity of s-SWCNTs is low compared to that of DGU.[20]

Conjugated polymers (poly(9,9-di-*n*-dodecylfluorenyl-2,7-diyl) and regioregular poly(3-dodecylthiophene-2,5-diyl) have been used for separation of s-SWCNTs, which are expensive than SWCNTs (Supporting Information, Table S1). Even after the separation, the polymer wrapped on s-SWCNTs has affected the electrical response of FETs, and the insulating polymers have to be removed.[21] The length of s-SWCNTs was also reduced after the sorting process. Selective chemistry separations were based on noncovalent adsorption of polymers on semiconducting nanotubes or preferential covalent attack on metallic nanotubes, and the latter one was more appealing as the associated separation process is usually rather simple.[22] Blanch et al.,[23] Schmidt et al.,[24] and Strano et al.,[25] have demonstrated that some water-soluble diazonium compounds, for example, 4-bromo-, 4-nitro-, 4-carboxy, and 4-chlorobenzenediazonium tetrafluoroborate, could preferentially extract electrons from m-SWCNTs rather than s-SWCNTs to form covalent −C−N bonds.

On the other hand, solution-derived s-SWCNT-based FETs showed poor performance when they were used as a random network film compared to perfectly aligned s-SWCNT arrays, having full surface coverage along with high density.[18,26] s-SWCNT alignment has been carried out using several methods such as Langmuir−Schaeffer deposition,[27] dielectrophoresis alignment,[28] Langmuir−Blodgett deposition,[29] filtration-based alignment,[30] spin-assisted alignment,[31] shear force alignment,[32] dimension-limited self-alignment,[10] and directional shrinking transfer alignment.[26] However, these aligned s-SWCNT array-based films showed low FET performances.[27−32] Thereby, Gopalan and Arnold et al. have developed a floating evaporative self-assembly method to align the s-SWCNTs with high density and quality on FETs to obtain high-performance devices.[33,34] Moreover, this method is unlikely suitable for wafer-scale fabrication of s-SWCNTs/FET and integrated circuits. Thus, there is a need for a universal, simple, and effective procedure to do the alignment of s-SWCNTs into arrays with high lengths and density.

In this study, s-SWCNTs were separated by mixing pristine (as-prepared) SWCNTs (AP-SWCNTs) with pluronic F-68 (PF-68) (Scheme 1a) by probe-assisted sonication (Scheme 1b) followed by standing the mixture for 1 day and then centrifuged to obtain monodispersed SWCNTs in the solution (Scheme 1b,c). The monodispersed SWCNTs were treated with para-amino diphenylamine diazonium sulfate (PADDS). PADDS was selectively reacted with m-SWCNTs and formed a stable −C−N bond on the m-SWCNT surface.[25] This selective functionalization of m-SWCNTs by PADDS made them denser than the unreacted or less-reacted s-SWCNTs and allowed them to settle during low-speed centrifugation.[23−25,35] UV−visible−near infrared (UV−vis−NIR), Raman, and Fourier-transform infrared (FT-IR) spectroscopy methods have been used to characterize the separated s-SWCNTs. UV−vis−NIR spectroscopy and Raman spectroscopy confirmed that the supernatant solution was enriched with s-SWCNTs, and the precipitate contained reacted m-SWCNTs. UV−vis−NIR showed that the purity of the separated s-SWCNTs was ~99.51%.

In addition to this, we have also demonstrated a simple method to produce highly aligned s-SWCNTs using the aqueous s-SWCNT solution under direct current(DC) electric field


https://dx.doi.org/10.1021/acsomega.0c04607
*ACS Omega* 2021, 6, 5146−5157

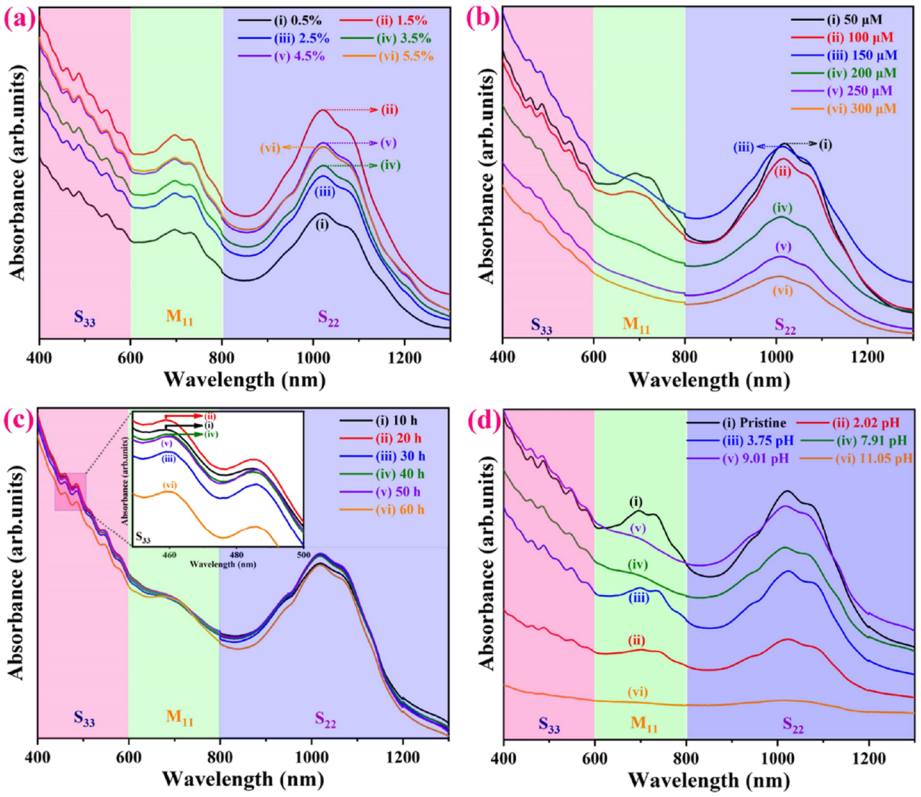


**Figure 1.** (a) UV−vis−NIR spectra for SWCNTs dispersed in PF-68 with different concentrations: (i) 0.5% to (vi) 5.5% PF-68, (b) SWCNTs dispersed in 1.5% PF-68 solutions were functionalized with different concentrations of PADDS after 40 h of treatment: (i) 50 to (vi) 300 $\mu$M PADDS, (c) SWCNTs dispersed in 1.5% PF-68 solutions were treated with 150 $\mu$M PADDS at different time intervals: (i) 10 to (vi) 60 h, and (d) SWCNTs dispersed in 1.5% PF-68 solutions were treated with 150 $\mu$M PADDS at different pH values after 20 h. All reactions were carried out at room temperature (27 ± 1 °C).

treatment. The aligned s-SWCNT arrays of nanotubes were deposited on FET devices by the drop-casting method to prepare about 30 devices with a channel length of 10 $\mu$m. The as-prepared s-SWCNTs/FET devices exhibited excellent performance with the field-effect mobility in the range of 4.5−30.4 $cm^2$/V.s and on−off ratios from $10^3$ to $10^4$ (for 30 devices). The DC electric field-aligned s-SWCNT arrays have successfully connected the microchannel of FETs as confirmed by field-emission scanning electron microscopy (FE-SEM) and switchable FETs.

## 2. RESULTS AND DISCUSSION

UV−vis−NIR spectroscopy was used to characterize the SWCNTs. The UV−vis−NIR spectrum could indicate the electronic transitions from the valence band (VB) to conduction band (CB) denoted as ($VB_n \rightarrow CB_n$), where n is the band index.[25] Figure 1a shows the $VB_1 \rightarrow CB_1$, first Van Hove transition of the metallic nanotubes ($M_{11}$) (armchair type) from 600 to 800 nm, as well as the Van Hove transitions of the $VB_2 \rightarrow CB_2$ ($S_{22}$) and $VB_3 \rightarrow CB_3$ ($S_{33}$) of semiconducting nanotubes (zigzag and chiral type) in the ranges from 800 to 1200 nm and 400 to 600 nm, respectively.[22,25] These absorption band regions could allow us to investigate the presence of metallic and semiconducting nanotube compositions in the separated dispersion.[25]After the treatment of SWCNTs with PADDS, because of high reactivity, preferentially metallic nanotubes were reacted with PADDS over seminanotubes under the optimized conditions (such as PADDS concentration, pH, and reaction time), and thereby electronic transition of metallic nanotubes was decreased in the region of 600−800 nm (Figure 1b-d).[23,25]

The dispersing ability of PF-68 was evaluated by preparing SWCNT dispersions using various concentrations of PF-68 (from 0.5 to 5.5%) with a fixed amount of as-prepared AP-SWCNTs at room temperature. All the mixtures were probe-sonicated followed by centrifugation, which produced monodispersed SWCNT solutions (Scheme 1, see Experimental Section 4). Next, UV−vis−NIR spectra of all monodispersed SWCNTs prepared with different concentrations of PF-68 were recorded (Figure 1a, curves i−vi). The dispersion obtained with 1.5% PF-68 showed well-resolved SWCNT bands in the UV−vis−NIR spectrum with high intensities (Figure 1a, curve ii).[23] Therefore, we selected 1.5% PF-68 solution as the optimum concentration to prepare monodispersed SWCNTs for further studies (Scheme S1).[23]

The selective metallic nanotube functionalization can be controlled by varying the PADDS concentration added into the monodispersed SWCNT solution. To study the effect of PADDS concentration, the selective reaction between PADDS and metallic nanotubes was carried out using different concentrations of PADDS from 50 to 300 $\mu$M at a fixed concentration of (0.25 mg $mL^{-1}$) monodispersed SWCNT solution.[23] After the reaction, the reacted SWCNTs were collected and centrifuged at 24,041 g for 180 min. The supernatant solution was analyzed by UV−vis−NIR spectroscopy. It was found that with the stepwise additions of PADDS into the monodispersed SWCNT solution, metallic tube functionalization was increased from 50 to 150 $\mu$M (Figure


https://dx.doi.org/10.1021/acsomega.0c04607
ACS Omega 2021, 6, 5146−5157

**Scheme 2. Schematic Representation of s-SWCNT Separation Using PADDS**[a]

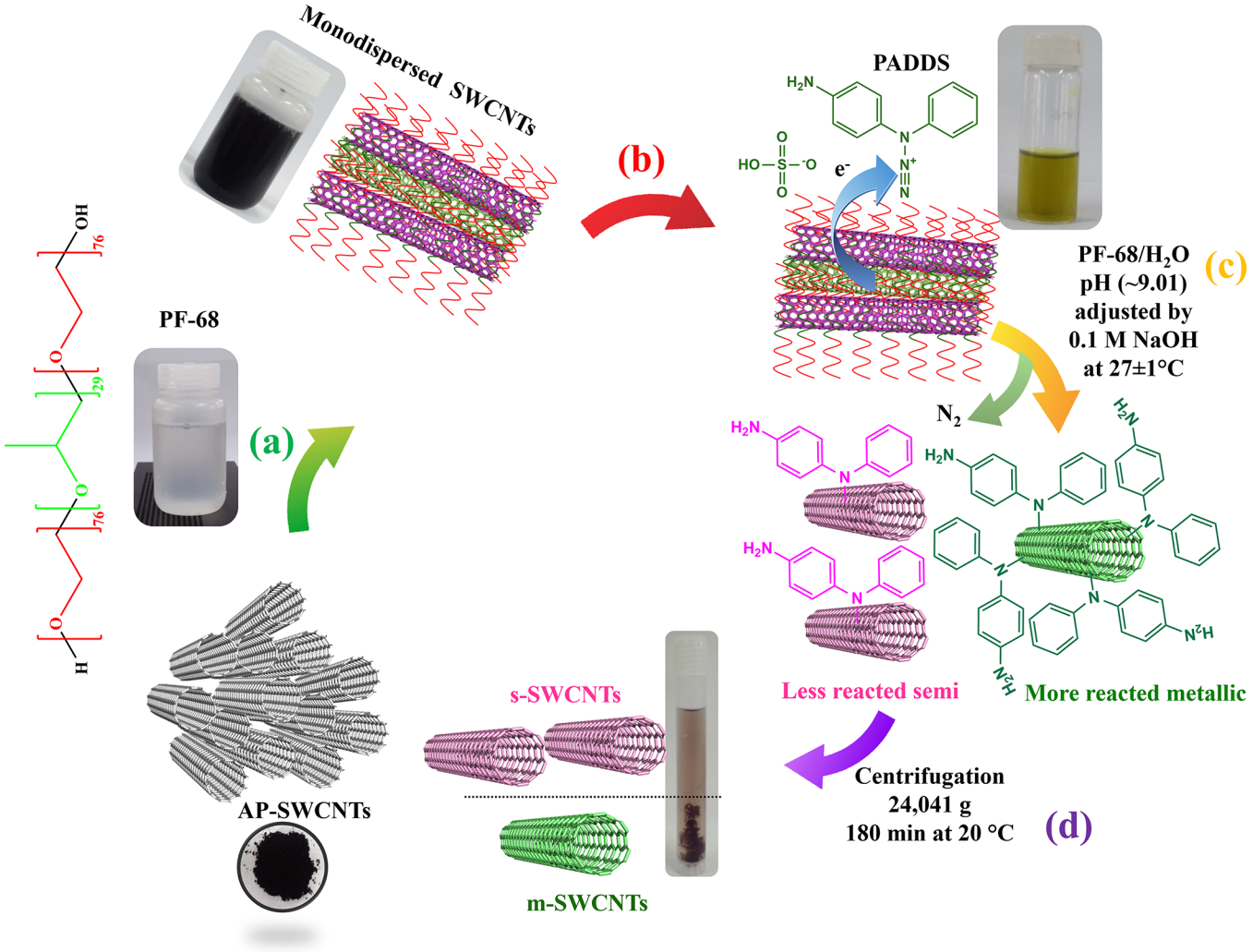


[a]The separation method starts from point (a), the preparation of the SWCNT dispersion in PF-68 surfactant solution, (b) covalent functionalization of as-produced SWCNTs, (c) PADDS-extracted electrons, thereby elimination of nitrogen ($N_2$) gas and formation of a stable −C−N covalent bond on the metallic nanotube surface, and (d) separation of unreacted/less reacted semiconducting SWCNTs. The chemical structure of PF-68 and PADDS is shown in steps 'a' and 'b'.

1b, curve i to iii). However, further increase of PADDS concentration from 200 to 300 $\mu$M added into monodispersed SWCNT solution (Figure 1b, curve iv to vi) did affect both the metallic and semiconducting absorbance regions, because of the excess concentration of PADDS which reacted with both types of nanotubes without any selectivity.[23,25,35] Based on the above results, the optimum concentration of PADDS was chosen as 150 $\mu$M for selective separation of m-SWCNTs from the s-SWCNTs (Figure 1b, curve iii).

Meanwhile, for the selective reaction, 10 $\mu$L of 10 mM PADDS was added 15 times to 10 mL of monodispersed SWCNTs (0.25 mg $mL^{-1}$) in 1.5% PF-68 and kept standing for 1 h and stirred using a magnetic bar at 1500 rpm up to 40 h at room temperature.[23] Under this condition, PADDS selectively extracts electrons from metallic nanotubes in the formation of a −C−N covalent bond with m-SWCNTs (Scheme 2a-c, see Experimental Section 4) and thereby demonstrates a highly chemo-selective reaction.[25] Therefore, we selected 150 $\mu$M PADDS as the optimum concentration to functionalize the metallic nanotubes over s-SWCNTs for further studies (Scheme S1).[23]

Next, the optimum reaction 'time' was evaluated by monitoring the reactions from 10 to 60 h with the addition of fixed concentration of PADDS into monodispersed SWCNT solution at room temperature. All the mixtures were stirred and centrifuged to collect the supernatant SWCNT solution (Scheme S1, see Experimental Section 4). After that, UV−vis−NIR spectra of all supernatant SWCNTs were measured (Figure 1c, curves i−vi). The semiconducting nanotubes were enriched in supernatant SWCNT solution, which was obtained from the reaction of 20 h. It showed well-resolved $S_{33}$ and $S_{22}$ bands in the UV−vis−NIR spectrum with high-intensity bands (Figure 1c, curve ii). Based on the above results, 20 h reaction time was selected as an optimum duration for the removal of the metallic nanotubes over semiconducting nanotubes from the monodispersed SWCNT solution (Scheme S1).[23]

To ascertain whether the selectivity of the reaction is pH-dependent or not, the reaction was carried out under different pH (from 2−11) solutions with the fixed time and concentration of PADDS (150 $\mu$M) in monodispersed SWCNT solution at room temperature. Subsequently, the mixtures were stirred and centrifuged to collect the supernatant SWCNT solutions


https://dx.doi.org/10.1021/acsomega.0c04607
ACS Omega 2021, 6, 5146−5157

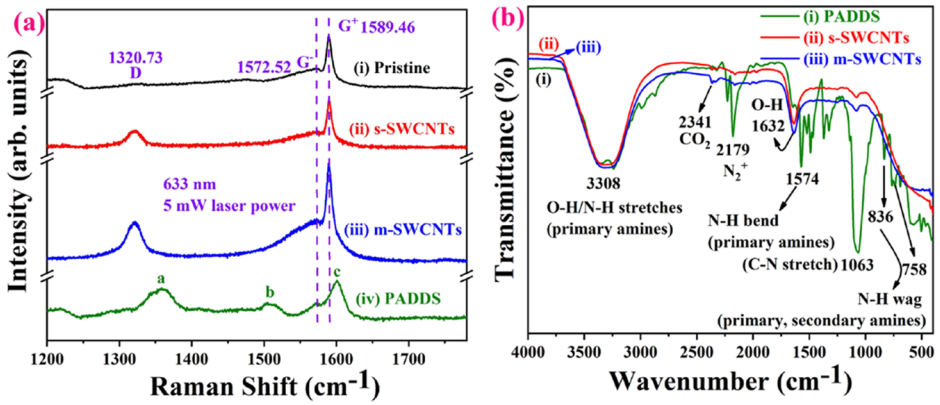


**Figure 2.** (a) Raman spectra of (i) pristine SWCNTs, (ii) supernatant s-SWCNTs, (iii) precipitated m-SWCNTs, and (iv) PADDS-mixed PF-68 aqueous solutions dried on a silica substrate and (b) FT-IR spectra of (i) PADDS aqueous solution, (ii) supernatant s-SWCNTs, and (iii) precipitated m-SWCNTs.

(Scheme S1, see Experimental Section 4). The variation in pH significantly influences the selectivity of metallic nanotube functionalization and removal as shown in Figure 1d, curves i to vi. The UV−vis−NIR spectrum has showed that metallic nanotubes were removed completely with the increase of pH from 7 to 9 and reached the maximum removal of metallic nanotubes at pH ∼9 (Table S2).[23,35] It was due to dediazoniation of PADDS under alkaline conditions (Scheme S2). During dediazoniation, PADDS was selectively reacted with m-SWCNTs (which has high density of electrons) and formed a stable −C−N covalent bond with the metallic nanotubes over semiconducting nanotubes (Scheme 2c-d).[23,25] The (4-aminophenyl)(phenyl)amide (decomposition product of PADDS) functionalized metallic nanotubes may now exist as the delocalized radical cation, which could further receive electrons from neighboring nanotubes or diazonium/sulfate.[23,25] Therefore, we attribute the changes in the UV−vis−NIR spectrum around 800 nm to a nonspecific solvatochromic shift that resulted from the addition of the sulfate counter ion.[26] However, under strong alkaline conditions (pH ∼11), the UV−vis−NIR bands of both seminanotubes and metallic nanotubes were completely suppressed, and it may be due to the aggregation effect of nanotubes along with (4-aminophenyl)-(phenyl)amide (Figure 1d, curve vi).[23,35] However, under acidic conditions (pH 2−4), the selective reaction on metallic nanotubes was not observed (Figure 1d, curves ii and iii) because of the poor reactivity of PADDS.[23] It was also confirmed that addition of NaOH was necessary to form (4-aminophenyl)-(phenyl)amide. Based on the above results, pH ∼9 was selected as an optimum pH to remove the metallic nanotubes by functionalization from s-SWCNTs. The possible mechanism of metallic nanotube functionalization by PADDS is shown in Scheme 2.[23−25,35−37]

To investigate about the decomposition pattern of PADDS, the dediazoniation reaction was carried out in the absence of SWCNTs and monitored by UV−vis spectroscopy (Figure S1). Fresh PADDS solution showed three absorption peaks at 246 (minor peak), 276 (shoulder peak), and 376 nm (strong peak) corresponding to the transitions of $\pi \rightarrow \pi^*$ aniline , $\pi \rightarrow \pi^*$ benzenoid, and $n \rightarrow \pi^*$ transition of diazonium (Figure S1, curve i).[38] However, after the treatment of 20 h in 1.5% PF-68 aqueous solution (pH ∼9), the decomposed PADDS solution was used to record the UV−vis spectrum (Figure S1, curve ii). It showed a peak at 276 nm because of the formation of (4-aminophenyl)(phenyl)amide from *N*-(4-iminocyclohexa-2,5-dien-1-ylidene)aniline.[38] It is worth noting that the diazonium peak completely disappeared because of dediazoniation of PADDS.[23,39,40] These results were also supported by the above mechanism as shown in Scheme 2c-d.[23,25]

Raman spectroscopy is an important nondestructive chemical analysis technique used to study the nanotube structure with unusual electronic and phonon properties of SWCNTs. The Raman spectra of pristine SWCNT (Figure 2a, curve i), s-SWCNT (Figure 2a, curve ii), m-SWCNT (Figure 2a, curve iii), and PADDS (Figure 2a, curve iv) samples were recorded using 633 nm laser excitation. The Raman spectrum of pristine SWCNTs and s-SWCNTs (Figure S2a) showed a clear radial breathing mode (RBM) peak between 100 and 300 $cm^{-1}$.[41] The lower frequency RBM range indicated two peaks at 155 $cm^{-1}$ (diameter ∼1.61 nm) and 171 $cm^{-1}$ (diameter ∼1.45 nm) because of the semiconducting zigzag and chiral nanotubes. Also, one small peak at 231 $cm^{-1}$ (diameter ∼1.06 nm) for metallic nanotubes (armchair) appeared for the pristine SWCNTs.[22,36] The diameters of individual nanotubes were calculated using the following equation $\omega$ (RBM) = (234/d + 10), where $\omega$ (RBM) represents the frequency of RBM mode ($cm^{-1}$) and d is the diameter of the nanotube (nm).[41]

We have also recorded the Raman spectrum of the pristine SWCNTs (Figure S2b, curve i) and separated s-SWCNT solution (Figure S2b, curve ii) using 785 nm (wavelength) laser excitation. As shown in Figure S2b, in the range from 100 to 300 $cm^{-1}$, a strong peak because of metallic nanotubes appeared at 162.31 $cm^{-1}$.[16,42] Interestingly, for the s-SWCNT solution, no metallic peak was observed, which may be due to the removal of m-SWCNTs by PADDS functionalization.[16,42] In addition, the disorder D-band peak was observed at 1320.73 $cm^{-1}$ with high intensity for m-SWCNTs compared to s-SWCNTs; this indicated the covalent functionalization ($sp^2$ C to $sp^3$ C) on the m-SWCNTs by the benzenoid groups as shown in Figure 2a.[25] At the same time, no significant D-band was observed at 1330 $cm^{-1}$ for pristine SWCNTs, which indicated that the defect-free nanotubes were used (Figure 2a, curve i).[23] The tangential modes in the range between 1450 and 1700 $cm^{-1}$ exhibited the electronic properties of nanotubes with their characteristic $G^-$ and $G^+$ features. For the pristine SWCNTs (Figure 2a, curve i), the $G^-$ band (at 1572.52 $cm^{-1}$) appeared as a broad and asymmetrical line of the Breit−Wigner−Fano peak was also observed because of the presence of metallic nanotubes. The $G^-$ band area in the s-SWCNT sample (Figure 2a, curve ii) was significantly smaller than that of pristine SWCNTs (Figure


https://dx.doi.org/10.1021/acsomega.0c04607
ACS Omega 2021, 6, 5146−5157

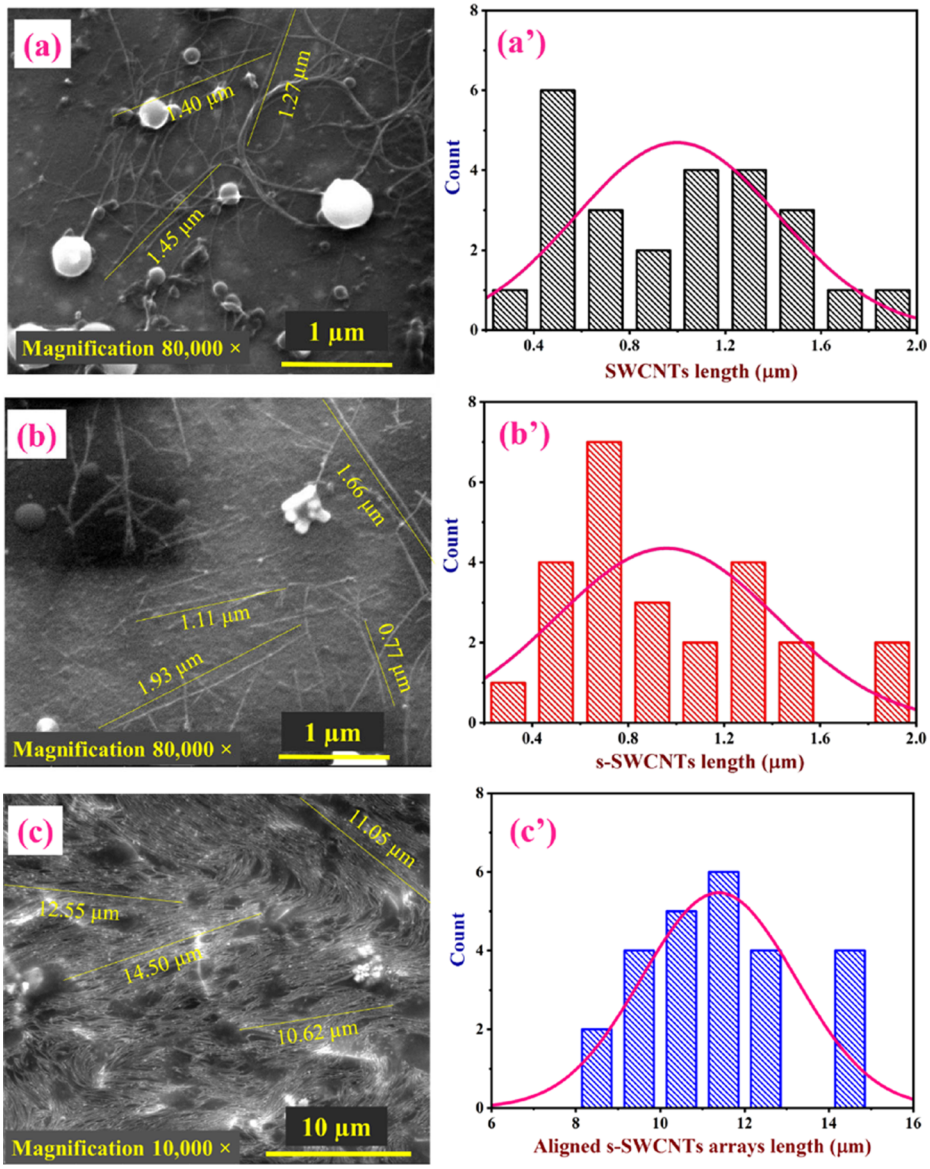


**Figure 3.** FE-SEM image of (a) pristine SWCNTs at 80,000× magnification with 1 $\mu$m scale bar and (a') histograms of the length distributions of nanotubes. (b) FE-SEM image of s-SWCNTs at 80,000× magnification with 1 $\mu$m scale bar and (b') histograms of the s-SWCNT length distributions. (c) FE-SEM image (at 10,000× with 10 $\mu$m scale bar) of aligned s-SWCNT arrays by DC electric field and (c') histograms of the overall lengths of aligned nanotube arrays and their distribution.

2a, curve i), proving that metallic nanotubes were removed from supernatant SWCNTs.[22,23,25,41] In addition, the Raman spectrum of the precipitated SWCNTs (Figure 2a, curve iii) showed a strong $G^-$ band, corroborating that this fraction contains enriched metallic nanotubes (Figure 2a).[25] Moreover, the Raman peaks of PADDS (Figure 2a, curve iv, peaks a to c and see Table S3 in the Supporting Information) completely disappeared after the reaction with SWCNTs.[43,44] These Raman results also supported the observation made by the UV−vis−NIR spectrum.

Next, the FT-IR spectrum was used to study the PADDS and PF-68 compounds. The FT-IR spectrum of the sample can be recorded by the absorption of IR frequencies by chemical bonds or functional groups, which lead to the fundamental vibrational and rotational or stretching and bending structures. FT-IR spectra of PADDS and PF-68 were recorded as shown in Figure 2b and Figure S2c. The FT-IR spectra of PADDS (Figure 2b, curve i) showed two N−H stretches between 3000 and 3600 $cm^{-1}$, which were attributed to surface primary amine groups of diazonium salt.[45] Similarly, primary amines were observed between 910 and 665 $cm^{-1}$.[45] The C−N stretch was recorded at lower wavenumbers (at 1063 $cm^{-1}$) because of PADDS as an aromatic compound.[45] Additionally, N−H bend was also noted at 1574 $cm^{-1}$.[45] The PADDS exhibited a transmittance peak of diazonium $N_2^+$ molecules at 2179 $cm^{-1}$.[46] Next, the FT-IR spectrum of the PF-68 polymer (Figure S2c) showed a small intense band at 3454 $cm^{-1}$ because of the vibrations of hydroxyl (−OH) groups.[47] A strong absorption band at 2883 $cm^{-1}$ was observed because of C−$CH_3$ stretching vibration of PF-68.[47] The characteristic peaks at 958 and 1096 $cm^{-1}$ in PF-68 were observed because of C−O symmetrical and asymmetrical stretching vibrations of ether groups. The peak at 1279 $cm^{-1}$ was assigned to −$CH_2$ group vibration of PF-68.[47] When we look at the FT-IR spectrum of s-SWCNTs (Figure 2b, curve ii) and m-SWCNTs (Figure 2b, curve iii), PADDS (Figure 2b,


https://dx.doi.org/10.1021/acsomega.0c04607
ACS Omega 2021, 6, 5146−5157

**Scheme 3. Schematic Representation of Alignment of s-SWCNTs Dispersed in 1.5% PF-68 under the DC Electric Field**

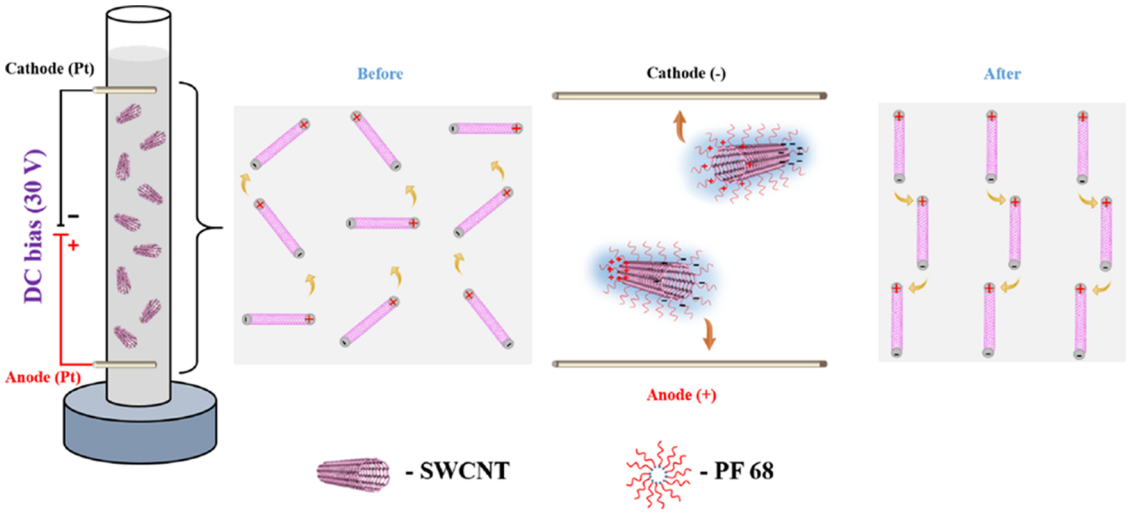


curve i) peaks completely disappeared after the reaction with SWCNTs.[45]

In the following section, we have discussed about the alignment of separated nanotubes (see Experimental Section 4). The aligned s-SWCNT arrays were characterized by FE-SEM. The surface morphologies and length of monodispersed SWCNTs (Figure 3a,a'), separated s-SWCNTs (Figure 3b,b'), and aligned s-SWCNT arrays of network (Figure 3c,c') deposited on (3-aminopropyl) triethoxysilane (APTES)-functionalized $SiO_2$/Si substrates were recorded as shown in Figure 3. Before the separation, the monodispersed SWCNTs resembled a random network with average tube (bundle) diameters of 10−30 nm with lengths of 0.2−2 $\mu$m (Figure 3a,a').[41] However, after the chemical reaction and separation, the separated s-SWCNTs had short lengths and low areal density as compared to the monodispersed SWCNTs (Figure 3b,b').[26]

Alignment of s-SWCNT arrays of network by a simple electric field method is carried out. The possible mechanism of s-SWCNT alignment under DC electric field is shown in Scheme 3.[48] Initially, the electric field effect induces the dipole moment at the edges of s-SWCNTs, which resulted in their rotation to a particular angle and then started to align under the electric field (see Experimental Section 4).[48] Finally, the polarized nanotubes were attracted to each other (head-to-head contact) and formed a chain-like structure in between the platinum anode and cathode (Scheme 3).[48,49] Scheme S3 (b) shows the details of the electric field-aligned nanotube array network deposition procedure (third step of Scheme S3 (a)). The aligned nanotube solution contains 1.5% PF-68. The hydrophobic polyoxypropylene chain of PF-68 adsorbs onto the nanotube surface by van der Waals force of attraction and hydrophilic polyoxyethylene chains exposed into the aqueous phase (Scheme 1).[23] When the electrically aligned nanotubes were drop-cast on the APTES-functionalized $SiO_2$/Si substrate, deposition of aligned nanotube arrays formed as a network onto the surface of the amino-functionalized $SiO_2$/Si substrate by the Coulombic force of attraction between the negatively charged −OH surface groups of s-SWCNTs and positively charged $-NH_2$ groups of the APTES-functionalized substrate (Scheme S3) (see Experimental Section 4).[50,51] The density of aligned nanotube arrays on the $SiO_2$/Si substrate can be readily controlled by adjusting the volume and dilution of the dispersion before the alignment. Under the present condition, aligned nanotube arrays were obtained with the length from 2 to 14 $\mu$m and the areal density varied from 2 to 20 nanotubes/$\mu$m (Figure 3c,c' and Figure S3) (Table 1).[49] As a control measure, UV−vis−NIR spectra of unaligned and aligned nanotube dispersions were recorded, which indicated that after the electric-field application, there were no changes in Van Hove transition of the aligned s-SWCNT solution (Figure S4).

**Table 1. Comparison of Lengths and Areal Densities of Aligned-s-SWCNTs, s-SWCNTs, and Pristine SWCNTs**

| s.no. | materials | lengths of nanotube arrays ($\mu$m)[a] | average length of nanotube arrays ($\mu$m) | areal density of nanotubes (tubes/$\mu$m) |
|---|---|---|---|---|
| 1 | pristine SWCNTs | 0.3−2.0 | 1.2 | 4−6 |
| 2 | s-SWCNTs | 0.3−2.0 | 0.8 | 2−4 |
| 3 | aligned-s-SWCNTs | 8−14 | 11 | 16−20 |

[a]Lengths of the nanotubes were measured using Image J software on the recorded FE-SEM images from Figure 3a-c. Pristine SWCNT lengths were calculated from Figure 3a. The s-SWCNT lengths were calculated from Figure 3b. Aligned-s-SWCNT array lengths were calculated from Figure 3c.

Finally, to test the electrical properties of the separated s-SWCNTs, electrically aligned s-SWCNT dispersion and pristine SWCNT (control) solution were drop-cast onto the channel of the FET devices to demonstrate the benefits of this separation and alignment. Figure 4(a,b) shows the schematic representation and optical image of the FET device (see Experimental Section 4). Figure 4(c−e) shows the p-type transistor behavior of the pristine SWCNT-modified FET and aligned s-SWCNT array (aligned s-SWCNT)-modified FETs under ambient conditions.[52] In fact, drain current of both devices increased when the negative gate voltage increased (Figure 4c,d). However, the pristine SWCNT-modified FET showed drain current saturation behavior than the aligned s-SWCNT-modified FET between +16 and −16 gate voltages.[13,52−54] Moreover, the following are the maximum drain currents of aligned s-SWCNTs/FET ($2.30 \times 10^{-4}$ A) and pristine SWCNTs/FET ($1.41 \times 10^{-4}$ A) observed at +2 drain voltage with (−16) gate voltage (Figure 4c,d).[9,13,22,52,54,55] Next, the


https://dx.doi.org/10.1021/acsomega.0c04607
ACS Omega 2021, 6, 5146−5157

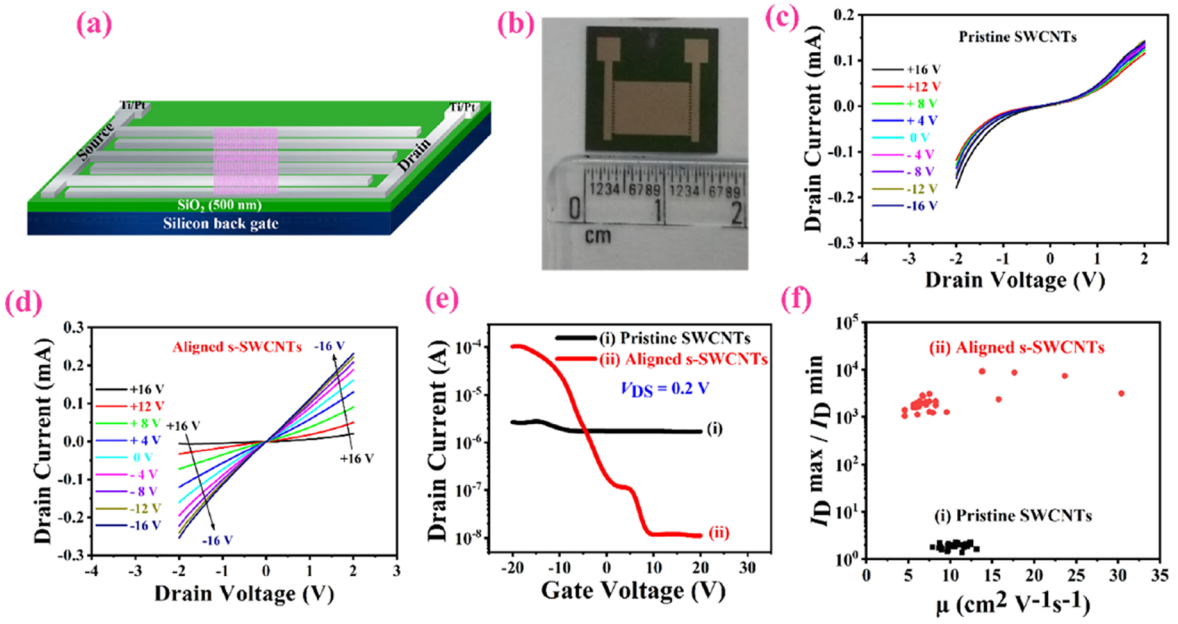


**Figure 4.** Schematic representation (a) and visual images of (b) back-gated s-SWCNTs/FET transistor with a scale. Output characteristic ($I_{DS} - V_{DS}$) curves of the as-prepared (c) pristine SWCNTs/FET and (d) aligned s-SWCNTs/FET. Both the curves were recorded from a drain voltage of −2 V to +2 V as a function of gate voltage swept between +16 V and −16 V in steps of 4 V. (e) Transfer characteristic ($I_{DS} - V_{GS}$) curves of the pristine SWCNTs/FET (i) and aligned s-SWCNTs/FET (ii) were measured at constant $V_{DS}$ bias (0.2 V). (f) Plots of on/off current ratios ($I_D^{max}/I_D^{min}$) vs field-effect mobility's ($\mu$) obtained from 30 individual devices.

**Table 2. Comparative Analysis of the Proposed Aligned s-SWCNTs/FET Transistor Performance with Other Sorted/Unsorted s-SWCNT-Based Thin-Film Transistors and FETs**

| chemicals used for sorting of s-SWCNTs | centrifugation method and speed | alignment or deposition method | channel length ($\mu$m) | mobility $\mu_{eff}$ ($cm^2\ V^{-1}\ s^{-1}$) | $\log_{10}$ ($I_{on}/I_{off}$) ratio | reference |
|---|---|---|---|---|---|---|
| poly(9-(1-octylonoyl)-9H-carbazole-2,7-diyl) | ultracentrifuge /40,000 g for 2 h | aerosol jet printing | 170 $\mu$m | 9.9 | 5 | 58 |
| 95% SWCNT aqueous solution was purchased from NanoIntegris | - | drop-casting | 160 $\mu$m | 7.5 | 4 | 59 |
| poly(9-(1-octylonoyl)-9H-carbazole-2,7-diyl) | ultracentrifuge20,000 g for 1 h | dip-coating | 5−50 $\mu$m | 28−67.5 | 5−6 | 1 |
| poly(3-dodecylthiophe-ne-2,5-diyl) | ultracentrifuge /3,67,000 g for 5 h | blade coating | 10 $\mu$m | 0.42−3.71 | 8 | 60 |
| PFO-BPy | ultracentrifuge /50,000 g for 1 h | DFES | 9 | 38 | 6 | 33 |
| PF-PD | ultracentrifuge /22,000 g for 0.5 h at 16 °C | drop-casting | 5−30 $\mu$m | 20−49 | 6 | 21 |
| PFO-BPy | ultracentrifuge /3,00,000 g for 1 h | FESA | 3 $\mu$m | 179 ± 10 | 5−7 | 34 |
| SDS | ultracentrifuge /2,87,700 g for 18 h | Langmuir − Schaefer | 120 nm | 130 ± 20 | 3 | 27 |
| 99% s-SWCNT aqueous solution was purchased from NanoIntegris | - | dielectrophoretic assembly | 2 $\mu$m | 16 | 2−4 | 61 |
| PADDS | centrifugation /24,041 g for 3 h | electric field alignment and drop-casting | 10 $\mu$m | 4.5−30.4 | 3−4 | this work |

field-effect mobility value was calculated for each FET transistor to observe how quickly an electron can move through a semiconductor when pulled by an electric field.[2] Figure 4e displays the drain current measurement as a function of gate voltage $V_{GS}$ (from −20 to +20) with an applied source-drain voltage, $V_{DS}$, of 0.2 V for aligned s-SWCNTs/FET and pristine SWCNTs/FET devices. For the devices made using the pristine SWCNT dispersion, the maximum field-effect mobility was found to be 13.1 $cm^2$/Vs.[56,57] However, after the separation of s-SWCNTs and electrical field alignment, the prepared devices showed a field-effect mobility of 30.4 $cm^2$/Vs, which is comparable to the performance of previously reported s-SWCNT/FETs (Table 2).[1,21,27,33,34,58−61] Similarly, on/off current ratios were calculated from the maximum drain current and minimum drain current divided in the gate voltage range of (−20 to +20 V). The $\log_{10}$ ($I_{on}/I_{off}$) current ratios were 3.96 and 0.35 for aligned s-SWCNTs/FET and pristine SWCNTs/FET, respectively. Figure 4f shows the plots of on/off current ratios vs field-effect mobility's of FETs fabricated using s-SWCNTs/FETs and pristine SWCNTs/FETs. It was found that the aligned s-SWCNT array-based FETs (about 30 devices) have exhibited higher field-effect mobility's and on/off current ratios than pristine SWCNT-based FETs.[9,13,54,60,62] The high performance of FETs was achieved because of the high-purity s-SWCNTs and the reduction in the number of random nanotube interactions on the FET channel by the DC electric field align-


https://dx.doi.org/10.1021/acsomega.0c04607
ACS Omega 2021, 6, 5146−5157

ment.[4,33,60,63,64] The random nanotube networks are known to be one of the important factors for the mobility losses and carrier trapping because of the intertube resistance. In particular, the polymers present on the nanotubes could act as an additional barrier to the hole transport through the channel.[19,60] Herein, our results have successfully demonstrated the effective uses of the separated and aligned s-SWCNTs to fabricate high-performance FETs.

## 3. CONCLUSIONS

We have reported a simple method for s-SWCNT separation using PADDS as the selective reagent. The proposed PADDS could selectively functionalize the metallic nanotubes over the semiconducting in monodispersed SWCNT solution. By this approach, we have easily separated the s-SWCNT solution with high purity up to ∼99.51% by low-speed centrifugation (24,041 g). The separation occurred because of charge transfer between PADDS and m-SWCNTs. The separation efficiency depends on the concentration of PADDS, reaction time, and solution pH. UV−vis−NIR and Raman spectroscopy methods have confirmed that s-SWCNT separation is achieved. Particularly, this selective chemistry-based s-SWCNT separation is beneficial for the chemical industry because it is inexpensive, there is no need to have sophisticated instruments, and so forth. Therefore, the cost of the separated s-SWCNT dispersion may decrease compared to commercially available in the market (Table S1). Moreover, we believe that this selective chemistry-based separation method may offer a large-scale production of s-SWCNTs. In addition, we have studied the alignment of nanotube arrays by DC electric field treatment. Finally, the electrical properties of the fabricated FETs proved the real application of separated and aligned s-SWCNT arrays compared to unseparated SWCNTs. The aligned s-SWCNT-based FET exhibited an on-state current of 110.25 $\mu$A ($V_{DS}$ = 0.2 V; $V_{GS}$ = −20 V), which is competitive to that of the reported s-SWCNT array-based FETs.[1,21,27,33,34,58−61] We believe that the reported electrically aligned s-SWCNT array-based FETs may be useful for the development of high-performance electronic devices.

## 4. EXPERIMENTAL SECTION

**4.1. Chemicals and Instruments.** Commercially available as-prepared AP-SWCNTs were purchased from carbon solutions, Inc., USA. PADDS salt was purchased from MP Biomedicals, LLC, France. PF-68 nonionic surfactant was purchased from Alfa Aesar, China, and APTES was purchased from Sigma-Aldrich, USA. All aqueous solutions were freshly prepared using doubly distilled water. The pH of the solutions was adjusted using 0.1 M HCl or 0.1 M NaOH to maintain different pH conditions. All the experiments were conducted at room temperature (27 ± 1 °C).

The electric field experiment was conducted using a DC power supply from Keithley (model: 2231A-30-3), USA. The absorption spectra of SWCNTs were measured using a UV−vis−NIR spectrophotometer, Agilent technologies (Cary 5000), USA. A micro-Raman spectrometer (LabRam HR evolution, Horiba) was used to characterize SWCNTs. The vibration and stretching modes of PF-68 and PADDS were analyzed using a FT-IR spectrometer (IRTracer-100, Shimadzu). The surface morphology of SWCNTs was analyzed using a field-emission scanning electron microscope (FE-SEM; model: Quanta 200 FEG) from FEI Netherlands. All electrical measurements were carried out using a semiconductor parameter analyzer (Keithley, model: 2612B, USA).

**4.2. Preparation of Monodispersed SWCNT Solution.** 25 mg of AP-SWCNTs was dispersed into 100 mL of PF-68 solution with different concentrations (0.5, 1.5, 2.5, 3.5, 4.5, and 5.5% PF-68 solution) via bath-sonication for 20 min (Labman Inc., Model: LMUC-2). The concentration of SWCNTs was 0.25 mg/mL in each aqueous solution. Next, these solutions were probe-sonicated (Pro 500, Labman) using a horn type probe (Titanium alloy, 6 mm diameter) for 60 min (3 sec ON/2 sec OFF) at 50% of amplitude (Figure S5). After the probe sonication, the resulting dispersion was centrifuged at 16,000 rpm (24,041 g) with a fixed angle rotor (C-24 Plus, Remi) for 90 min to precipitate the bundles and impurities. Then, the monodispersed SWCNT solution was filtered through a Whatman filter paper (pore size of 11 $\mu$m) to remove the bundles and impurities. Finally, the collected monodispersed SWCNT solution was utilized for s-SWCNT separation (Scheme 1).

**4.3. Separation of s-SWCNTs.** The separation of s-SWCNTs was carried out by changing various parameters such as concentrations of PF-68 and PADDS with reaction time and solution pH (Scheme S1). The batch mode technique was carried out by stirring with an optimized amount of the PADDS in 10 mL of the monodispersed SWCNT solution. After the reaction with PADDS, the suspensions were centrifuged at 24,041 g for 180 min to remove the precipitate/bundles, and 80% of the supernatant was collected from the centrifuge tube. The pH of the solutions was adjusted using 0.1 M of HCl or NaOH solutions. The effects of pH (2−11), monodispersed SWCNT solution concentration (0.25 mg/mL), PF-68 surfactant concentration (0.5 to 5.5%), initial PADDS concentration (50−300 $\mu$M), and effect of time (10−60 h) were optimized for the effective separation (Scheme S1 and Figure 1). The length and density of s-SWCNTs before and after the electrical field alignment were determined through FE-SEM. For this purpose, FE-SEM micrographs were analyzed using the Java-based image processing program known as Image J software.[65]

**4.4. Alignment of s-SWCNTs.** The separated s-SWCNT solution was then transferred into a 10 mL electric field cell where two platinum electrodes were placed on the lower and upper side as an anode and cathode, respectively. Next, 30 V was applied through the Pt electrodes using a DC power supply (for 6 h) (Scheme 3). After applying the electric field, the alignment of the s-SWCNTs was compared with that of s-SWCNTs and pristine SWCNTs by FE-SEM (Scheme 3 and Figure 3).

**4.5. Fabrication of s-SWCNTs/FET Devices.** To prove the benefits of this separation and alignment of s-SWCNTs, FETs were fabricated with aligned s-SWCNT arrays and pristine SWCNTs (fabricated from the monodispersed SWCNT solution). All FETs were fabricated on p-type silicon (Si) wafer (diameter: 7.62 cm, thickness: 375 $\mu$m, polished: single side, orientation: <100>, and resistivity: 1−10 Ω cm) deposited by a silicon dioxide ($SiO_2$) layer (500 nm) as a gate dielectric. Then, electrical contacts were made by Ti/Pt evaporation (source and drain electrodes) through a metal mask.[54] The fabricated FET channel length and width were 10 and 200 $\mu$m, respectively. Finally, a disco automatic dicing saw instrument (DAD 322, diamond blade, 22,000 RPM) was used to dice the wafer into smaller dies 1.6 cm × 1.6 cm. Next, the fabricated FET devices were functionalized by APTES prior to SWCNT deposition.[54] To place nanotubes on the channel, the APTES-


https://dx.doi.org/10.1021/acsomega.0c04607
ACS Omega 2021, 6, 5146−5157

functionalized FET devices were drop-cast by 100 $\mu$L of aligned s-SWCNT or pristine SWCNT solution, and dried at room temperature for 12 h. After fabricating the dried nanotube film on the channel of the FET, it was washed with distilled water and heat-treated at 200 °C for two hours to remove the surfactants and decrease the contact resistance.[54] Finally, the fabricated s-SWCNTs/FETs (using aligned nanotubes) and pristine SWCNTs/FETs were tested by electrical measurements. The field-effect mobility was calculated according to the following equation.[62]

$$\mu_{\text{eff}} \equiv \frac{\left(\frac{dI}{dV_g}\right) L_{\text{ox}}\, L_{\text{sd}}}{\varepsilon\, W_{\text{sd}}\, V_{\text{sd}}}$$

$$= \frac{0.81\ \frac{\mu A}{V} \times 500\ \text{nm} \times 10\ \mu\text{m}}{3.9 \times 8.85 \times 10^{-12}\ \frac{F}{m} \times 200\ \mu\text{m} \times 200\ mV} = 30.40\ \frac{\text{cm}^2}{Vs}$$

Where $\mu_{\text{eff}}$ is the effective field-effect mobility, $L_{\text{ox}}$ is the thickness of the gate oxide, $V_{\text{sd}}$ is the source-drain voltage, $W_{\text{sd}}$ is the channel width, $\varepsilon$ is the dielectric constant of the gate oxide, $L_{\text{sd}}$ is the channel length, and $dI/dV_{\text{g}}$ is the transconductance.

## ■ ASSOCIATED CONTENT

### Supporting Information

The Supporting Information is available free of charge at https://pubs.acs.org/doi/10.1021/acsomega.0c04607.

UV−vis−NIR characterization, purity calculations of pristine SWCNTs and s-SWCNTs from the UV−vis−NIR spectrum, optimized conditions for the s-SWCNT separation process, dediazoniation of PADDS in 1.5% PF-68 aqueous solution (pH ∼ 9), schematic illustration of the alignment of s-SWCNT arrays during the deposition procedure by the drop-casting method, UV−vis absorbance spectra of PADDS (150 $\mu$M) in 1.5% PF-68 aqueous solution (pH ∼9): (i) before 0 h (ii) after 20 h, Raman spectra of (i) pristine SWCNTs and (ii) supernatant s-SWCNTs recorded using (a) 633 nm laser excitation and (b) 785 nm laser excitation, (c) FT-IR spectra of PF-68 polymer, FE-SEM image of the aligned s-SWCNT array network by electric field at 80,000× magnification with 1 $\mu$m scale bar, UV−vis−NIR spectra of (i) pristine SWCNT, (ii) s-SWCNT, and (iii) aligned s-SWCNT dispersions, (a) photographs of different concentrations of PF-68 aqueous solutions and (b) pristine SWCNTs dispersed in different concentrations of PF-68 aqueous solutions, comparison of SWCNTs' price and polymers used for the separation, calculated semiconducting percentages in the pristine SWCNTs and separated s-SWCNT dispersions, and Raman vibrational bands of PADDS and their assignments (PDF).

## ■ AUTHOR INFORMATION


### Corresponding Author

**Ashok K. Sundramoorthy** − *Department of Chemistry, SRM Institute of Science and Technology, Kattankulathur 603203, Tamil Nadu, India;* orcid.org/0000-0002-8512-9393; Email: ashokkus@srmist.edu.in

### Authors

**Thomaati Haridass Vignesh Kumar** − *Department of Chemistry, SRM Institute of Science and Technology, Kattankulathur 603203, Tamil Nadu, India*

**Jerome Rajendran** − *Department of Chemistry, SRM Institute of Science and Technology, Kattankulathur 603203, Tamil Nadu, India*

**Ramila D. Nagarajan** − *Department of Chemistry, SRM Institute of Science and Technology, Kattankulathur 603203, Tamil Nadu, India*

**Gayathri Jeevanandam** − *Department of Chemistry, SRM Institute of Science and Technology, Kattankulathur 603203, Tamil Nadu, India*

**Anatoly N. Reshetilov** − *G.K. Skryabin Institute of Biochemistry and Physiology of Microorganisms of the Russian Academy of Sciences (IBPM RAS), Subdivision of "Federal Research Center Pushchino Biological Research Center of the Russian Academy of Sciences"(FRC PBRC RAS), 142290 Moscow, Russia*

Complete contact information is available at: https://pubs.acs.org/10.1021/acsomega.0c04607


### Notes

The authors declare no competing financial interest.

## ■ ACKNOWLEDGMENTS

This work was financially supported by the Department of Science and Technology (DST)-Science and Engineering Research Board (SERB), Government of India for the funding through Early Career Research Award (Ref. No.: ECR/2016/001446), and Department of Science and Technology (International Bilateral Cooperation Division) for financial support through "INDO-RUSSIA Project (No. INT/RUS/RFBR/385)". The FET devices were fabricated using the facilities at The National Nanofabrication Centre (NNFC) from Centre for Nano Science and Engineering (CeNSE) department in Indian Institute of Science, Bengaluru. We thank the SRM Institute of Science and Technology for providing laboratory and instrument facilities to carry out this research project.

## ■ ABBREVIATIONS

| | |
|---|---|
| DFES | dose-controlled floating evaporative self-assembly |
| FESA | floating evaporative self-assembly |
| PFO-BPy | poly[(9,9-dioctylfluo-renyl-2,7-diyl)-alt-co-(6,6′-{2,2′- bipyridine})] |
| PF-PD | poly[(9,9-di-n-dodecyl-2,7-fluroen-diyldimethine)-(1,4-phenylenedinitrilo-methine)] and |
| SDS | sodium dodecyl sulfate. |

## ■ REFERENCES


(1) Gu, J.; Han, J.; Liu, D.; Yu, X.; Kang, L.; Qiu, S.; Jin, H.; Li, H.; Li, Q.; Zhang, J. Solution-Processable High-Purity Semiconducting SWCNTs for Large-Area Fabrication of High-Performance Thin-Film Transistors. *Small* **2016**, *12*, 4993−4999.

(2) Bati, A. S. R.; Yu, L.; Batmunkh, M.; Shapter, J. G. Recent Advances in Applications of Sorted Single-Walled Carbon Nanotubes. *Adv. Funct. Mater.* **2019**, *29*, No. 1902273.

(3) Bishop, M. D.; Hills, G.; Srimani, T.; Lau, C.; Murphy, D.; Fuller, S.; Humes, J.; Ratkovich, A.; Nelson, M.; Shulaker, M. M. Fabrication of Carbon Nanotube Field-Effect Transistors in Commercial Silicon Manufacturing Facilities. *Nat. Electron.* **2020**, *3*, 492−501.

(4) Cao, Y.; Brady, G. J.; Gui, H.; Rutherglen, C.; Arnold, M. S.; Zhou, C. Radio Frequency Transistors Using Aligned Semiconducting

Carbon Nanotubes with Current-Gain Cutoff Frequency and Maximum Oscillation Frequency Simultaneously Greater than 70 GHz. *ACS Nano* **2016**, *10*, 6782−6790.
(5) Liu, L.; Ding, L.; Zhong, D.; Han, J.; Wang, S.; Meng, Q.; Qiu, C.; Zhang, X.; Peng, L.-M.; Zhang, Z. Carbon Nanotube Complementary Gigahertz Integrated Circuits and Their Applications on Wireless Sensor Interface Systems. *ACS Nano* **2019**, *13*, 2526−2535.
(6) Zhu, M.; Zhang, Z.; Peng, L. High-Performance and Radiation-Hard Carbon Nanotube Complementary Static Random-Access Memory. *Adv. Electron. Mater.* **2019**, *5*, No. 1900313.
(7) Blackburn, J. L. Semiconducting Single-Walled Carbon Nanotubes in Solar Energy Harvesting. *ACS Energy Lett.* **2017**, *2*, 1598−1613.
(8) Schroeder, V.; Savagatrup, S.; He, M.; Lin, S.; Swager, T. M. Carbon Nanotube Chemical Sensors. *Chem. Rev.* **2019**, *119*, 599−663.
(9) Kumar, T. H. V.; Raman Pillai, S. K.; Chan-Park, M. B.; Sundramoorthy, A. K. Highly Selective Detection of an Organophosphorus Pesticide, Methyl Parathion, Using Ag−ZnO−SWCNT Based Field-Effect Transistors. *J. Mater. Chem. C* **2020**, *8*, 8864−8875.
(10) Liu, L.; Han, J.; Xu, L.; Zhou, J.; Zhao, C.; Ding, S.; Shi, H.; Xiao, M.; Ding, L.; Ma, Z. Aligned, High-Density Semiconducting Carbon Nanotube Arrays for High-Performance Electronics. *Science* **2020**, *368*, 850−856.
(11) Cui, J.; Su, W.; Yang, D.; Li, S.; Wei, X.; Zhou, N.; Zhou, W.; Xie, S.; Kataura, H.; Liu, H. Mass Production of High-Purity Semiconducting Carbon Nanotubes by Hydrochloric Acid Assisted Gel Chromatography. *ACS Appl. Nano Mater.* **2019**, *2*, 343−350.
(12) Tyler, T. P.; Shastry, T. A.; Leever, B. J.; Hersam, M. C. Narrow Diameter Distributions of Metallic Arc Discharge Single-Walled Carbon Nanotubes via Dual-Iteration Density Gradient Ultracentrifugation. *Adv. Mater.* **2012**, *24*, 4765−4768.
(13) Ihara, K.; Numata, H.; Nihey, F.; Yuge, R.; Endoh, H. High Purity Semiconducting Single-Walled Carbon Nanotubes for Printed Electronics. *ACS Appl. Nano Mater.* **2019**, *2*, 4286−4292.
(14) Kuwahara, Y.; Sasaki, F.; Saito, T. Environment Effects on the Charge States of Metallic and Semiconducting SWCNTs during Their Separation by the Electric-Field Induced Layer Formation Method. *J. Phys. Chem. C* **2019**, *123*, 3829−3835.
(15) Fagan, J. A.; Hároz, E. H.; Ihly, R.; Gui, H.; Blackburn, J. L.; Simpson, J. R.; Lam, S.; Hight Walker, A. R.; Doorn, S. K.; Zheng, M. Isolation Of> 1 Nm Diameter Single-Wall Carbon Nanotube Species Using Aqueous Two-Phase Extraction. *ACS Nano* **2015**, *9*, 5377−5390.
(16) Wang, J.; Nguyen, T. D.; Cao, Q.; Wang, Y.; Tan, M. Y. C.; Chan-Park, M. B. Selective Surface Charge Sign Reversal on Metallic Carbon Nanotubes for Facile Ultrahigh Purity Nanotube Sorting. *ACS Nano* **2016**, *10*, 3222−3232.
(17) Ao, G.; Streit, J. K.; Fagan, J. A.; Zheng, M. Differentiating Left- and Right-Handed Carbon Nanotubes by DNA. *J. Am. Chem. Soc.* **2016**, *138*, 16677−16685.
(18) Qiu, S.; Wu, K.; Gao, B.; Li, L.; Jin, H.; Li, Q. Solution-Processing of High-Purity Semiconducting Single-Walled Carbon Nanotubes for Electronics Devices. *Adv. Mater.* **2019**, *31*, No. 1800750.
(19) Lei, T.; Pochorovski, I.; Bao, Z. Separation of Semiconducting Carbon Nanotubes for Flexible and Stretchable Electronics Using Polymer Removable Method. *Acc. Chem. Res.* **2017**, *50*, 1096−1104.
(20) Um, J.-E.; Song, S. G.; Yoo, P. J.; Song, C.; Kim, W.-J. Large-Scale Separation of Single-Walled Carbon Nanotubes by Electronic Type Using Click Chemistry. *Appl. Surf. Sci.* **2018**, *429*, 278−283.
(21) Lei, T.; Chen, X.; Pitner, G.; Wong, H.-S. P.; Bao, Z. Removable and Recyclable Conjugated Polymers for Highly Selective and High-Yield Dispersion and Release of Low-Cost Carbon Nanotubes. *J. Am. Chem. Soc.* **2016**, *138*, 802−805.
(22) Sundramoorthy, A. K.; Mesgari, S.; Wang, J.; Kumar, R.; Sk, M. A.; Yeap, S. H.; Zhang, Q.; Sze, S. K.; Lim, K. H.; Chan-Park, M. B. Scalable and Effective Enrichment of Semiconducting Single-Walled Carbon Nanotubes by a Dual Selective Naphthalene-Based Azo Dispersant. *J. Am. Chem. Soc.* **2013**, *135*, 5569−5581.
(23) Blanch, A. J.; Lenehan, C. E.; Quinton, J. S. Dispersant Effects in the Selective Reaction of Aryl Diazonium Salts with Single-Walled Carbon Nanotubes in Aqueous Solution. *J. Phys. Chem. C* **2012**, *116*, 1709−1723.
(24) Schmidt, G.; Filoramo, A.; Derycke, V.; Bourgoin, J.; Chenevier, P. Labile Diazo Chemistry for Efficient Silencing of Metallic Carbon Nanotubes. *Chem. − Eur. J.* **2011**, *17*, 1415−1418.
(25) Strano, M. S.; Dyke, C. A.; Usrey, M. L.; Barone, P. W.; Allen, M. J.; Shan, H.; Kittrell, C.; Hauge, R. H.; Tour, J. M.; Smalley, R. E. Electronic Structure Control of Single-Walled Carbon Nanotube Functionalization. *Science* **2003**, *301*, 1519−1522.
(26) Zhu, M.; Si, J.; Zhang, Z.; Peng, L. Aligning Solution-Derived Carbon Nanotube Film with Full Surface Coverage for High-Performance Electronics Applications. *Adv. Mater.* **2018**, *30*, No. 1707068.
(27) Cao, Q.; Han, S.; Tulevski, G. S.; Zhu, Y.; Lu, D. D.; Haensch, W. Arrays of Single-Walled Carbon Nanotubes with Full Surface Coverage for High-Performance Electronics. *Nat. Nanotechnol.* **2013**, *8*, 180.
(28) Shekhar, S.; Stokes, P.; Khondaker, S. I. Ultrahigh Density Alignment of Carbon Nanotube Arrays by Dielectrophoresis. *ACS Nano* **2011**, *5*, 1739−1746.
(29) Giancane, G.; Ruland, A.; Sgobba, V.; Manno, D.; Serra, A.; Farinola, G. M.; Omar, O. H.; Guldi, D. M.; Valli, L. Aligning Single-Walled Carbon Nanotubes By Means Of Langmuir−Blodgett Film Deposition: Optical, Morphological, and Photo-Electrochemical Studies. *Adv. Funct. Mater.* **2010**, *20*, 2481−2488.
(30) He, X.; Gao, W.; Xie, L.; Li, B.; Zhang, Q.; Lei, S.; Robinson, J. M.; Hároz, E. H.; Doorn, S. K.; Wang, W. Wafer-Scale Monodomain Films of Spontaneously Aligned Single-Walled Carbon Nanotubes. *Nat. Nanotechnol.* **2016**, *11*, 633.
(31) LeMieux, M. C.; Roberts, M.; Barman, S.; Jin, Y. W.; Kim, J. M.; Bao, Z. Self-Sorted, Aligned Nanotube Networks for Thin-Film Transistors. *Science* **2008**, *321*, 101−104.
(32) Park, S.; Pitner, G.; Giri, G.; Koo, J. H.; Park, J.; Kim, K.; Wang, H.; Sinclair, R.; Wong, H. P.; Bao, Z. Large-Area Assembly of Densely Aligned Single-Walled Carbon Nanotubes Using Solution Shearing and Their Application to Field-Effect Transistors. *Adv. Mater.* **2015**, *27*, 2656−2662.
(33) Joo, Y.; Brady, G. J.; Arnold, M. S.; Gopalan, P. Dose-Controlled, Floating Evaporative Self-Assembly and Alignment of Semiconducting Carbon Nanotubes from Organic Solvents. *Langmuir* **2014**, *30*, 3460−3466.
(34) Brady, G. J.; Joo, Y.; Wu, M.-Y.; Shea, M. J.; Gopalan, P.; Arnold, M. S. Polyfluorene-Sorted, Carbon Nanotube Array Field-Effect Transistors with Increased Current Density and High on/off Ratio. *ACS Nano* **2014**, *8*, 11614−11621.
(35) Kim, W.-J.; Usrey, M. L.; Strano, M. S. Selective Functionalization and Free Solution Electrophoresis of Single-Walled Carbon Nanotubes: Separate Enrichment of Metallic and Semiconducting SWNT. *Chem. Mater.* **2007**, *19*, 1571−1576.
(36) Wang, C.; Xu, W.; Zhao, J.; Lin, J.; Chen, Z.; Cui, Z. Selective Silencing of the Electrical Properties of Metallic Single-Walled Carbon Nanotubes by 4-Nitrobenzenediazonium Tetrafluoroborate. *J. Mater. Sci.* **2014**, *49*, 2054−2062.
(37) Schmidt, G.; Gallon, S.; Esnouf, S.; Bourgoin, J.; Chenevier, P. Mechanism of the Coupling of Diazonium to Single-Walled Carbon Nanotubes and Its Consequences. *Chem. − Eur. J.* **2009**, *15*, 2101−2110.
(38) Thompson, J. O. F.; Saalbach, L.; Crane, S. W.; Paterson, M. J.; Townsend, D. Ultraviolet Relaxation Dynamics of Aniline, N, N-Dimethylaniline and 3, 5-Dimethylaniline at 250 Nm. *J. Chem. Phys.* **2015**, *142*, 114309.
(39) Perkampus, H.-H. *UV-VIS Spectroscopy and Its Applications*; Springer Science & Business Media, 2013.
(40) Zhang, J.; Men, Y.; Lv, S.; Yi, L.; Chen, J.-F. Protein Tetrazinylation via Diazonium Coupling for Covalent and Catalyst-Free Bioconjugation. *Org. Biomol. Chem.* **2015**, *13*, 11422−11425.
(41) Kumar, T. H. V.; Sundramoorthy, A. K. Electrochemical Biosensor for Methyl Parathion Based on Single-Walled Carbon Nanotube/Glutaraldehyde Crosslinked Acetylcholinesterase-Wrapped


https://dx.doi.org/10.1021/acsomega.0c04607
*ACS Omega* 2021, 6, 5146−5157

Bovine Serum Albumin Nanocomposites. *Anal. Chim. Acta* **2019**, *1074*, 131−141.
(42) Wang, C.; Qian, L.; Xu, W.; Nie, S.; Gu, W.; Zhang, J.; Zhao, J.; Lin, J.; Chen, Z.; Cui, Z. High Performance Thin Film Transistors Based on Regioregular Poly (3-Dodecylthiophene)-Sorted Large Diameter Semiconducting Single-Walled Carbon Nanotubes. *Nanoscale* **2013**, *5*, 4156−4161.
(43) Zhang, X.; Rösicke, F.; Syritski, V.; Sun, G.; Reut, J.; Hinrichs, K.; Janietz, S.; Rappich, J. Influence of the Para-Substitutent of Benzene Diazonium Salts and the Solvent on the Film Growth during Electrochemical Reduction. *Zeitschrift für Phys. Chemie* **2014**, *228*, 557−573.
(44) Betelu, S.; Tijunelyte, I.; Boubekeur-Lecaque, L.; Ignatiadis, I.; Ibrahim, J.; Gaboreau, S.; Berho, C.; Toury, T.; Guenin, E.; Lidgi-Guigui, N.; et al. Evidence of the Grafting Mechanisms of Diazonium Salts on Gold Nanostructures. *J. Phys. Chem. C* **2016**, *120*, 18158−18166.
(45) IR Spectroscopy Tutorial: Amines http://www.orgchemboulder.com/Spectroscopy/irtutor/aminesir.shtml.
(46) Girard, H. A.; Petit, T.; Perruchas, S.; Gacoin, T.; Gesset, C.; Arnault, J. C.; Bergonzo, P. Surface Properties of Hydrogenated Nanodiamonds: A Chemical Investigation. *Phys. Chem. Chem. Phys.* **2011**, *13*, 11517−11523.
(47) Seema, S.; Datta, M. Organoclay Pluronic F68−Montmorillonite, as a Sustained Release Drug Delivery Vehicle for Propranolol Hydrochloride. *Eur. Chem. Bull.* **2014**, *3*, 593−604.
(48) Amani, A. M.; Hashemi, S. A.; Mousavi, S. M.; Abrishamifar, S. M.; Vojood, A. Electric Field Induced Alignment of Carbon Nanotubes: Methodology and Outcomes. In *Carbon nanotubes-recent progress*; IntechOpen, 2017.
(49) Ma, C.; Zhu, Y.; Yang, X.; Ji, L.; Zhang, C.; Liang, J. Macroscopic Networks of Carbon Nanotubes in PMMA Matrix Induced by AC Electric Field. *J. Dispersion Sci. Technol.* **2008**, *29*, 502−507.
(50) Sarkar, A.; Daniels-Race, T. Electrophoretic Deposition of Carbon Nanotubes on 3-Amino-Propyl-Triethoxysilane (APTES) Surface Functionalized Silicon Substrates. *Nanomaterials* **2013**, *3*, 272−288.
(51) Wang, Y.; Pillai, S. K. R.; Chan-Park, M. B. High-Performance Partially Aligned Semiconductive Single-walled Carbon Nanotube Transistors Achieved with a Parallel Technique. *Small* **2013**, *9*, 2960−2969.
(52) Voggu, R.; Rao, K. V.; George, S. J.; Rao, C. N. R. A Simple Method of Separating Metallic and Semiconducting Single-Walled Carbon Nanotubes Based on Molecular Charge Transfer. *J. Am. Chem. Soc.* **2010**, *132*, 5560−5561.
(53) Ghosh, S.; Rao, C. N. R. Separation of Metallic and Semiconducting Single-Walled Carbon Nanotubes through Fluorous Chemistry. *Nano Res.* **2009**, *2*, 183−191.
(54) Ihara, K.; Endoh, H.; Saito, T.; Nihey, F. Separation of Metallic and Semiconducting Single-Wall Carbon Nanotube Solution by Vertical Electric Field. *J. Phys. Chem. C* **2011**, *115*, 22827−22832.
(55) Maeda, Y.; Kimura, S.; Kanda, M.; Hirashima, Y.; Hasegawa, T.; Wakahara, T.; Lian, Y.; Nakahodo, T.; Tsuchiya, T.; Akasaka, T. Large-Scale Separation of Metallic and Semiconducting Single-Walled Carbon Nanotubes. *J. Am. Chem. Soc.* **2005**, *127*, 10287−10290.
(56) Burghard, M.; Klauk, H.; Kern, K. Carbon-based Field-effect Transistors for Nanoelectronics. *Adv. Mater.* **2009**, *21*, 2586−2600.
(57) Cao, Q.; Kim, H.; Pimparkar, N.; Kulkarni, J. P.; Wang, C.; Shim, M.; Roy, K.; Alam, M. A.; Rogers, J. A. Medium-Scale Carbon Nanotube Thin-Film Integrated Circuits on Flexible Plastic Substrates. *Nature* **2008**, *454*, 495−500.
(58) Wang, X.; Wei, M.; Li, X.; Shao, S.; Ren, Y.; Xu, W.; Li, M.; Liu, W.; Liu, X.; Zhao, J. Large-Area Flexible Printed Thin-Film Transistors with Semiconducting Single-Walled Carbon Nanotubes for NO2 Sensors. *ACS Appl. Mater. Interfaces* **2020**, *12*, 51797−51807.
(59) Park, B.; Jang, J.; Kim, H.; Seo, J.; Yoo, H.; Kim, T.; Hong, Y. Dense Assembly of Finely Patterned Semiconducting Single-Walled Carbon Nanotubes via a Selective Transfer Method of Nanotube-Attracting Layers. *ACS Appl. Mater. Interfaces* **2020**, *12*, 38441−38450.
(60) Derenskyi, V.; Gomulya, W.; Rios, J. M. S.; Fritsch, M.; Fröhlich, N.; Jung, S.; Allard, S.; Bisri, S. Z.; Gordiichuk, P.; Herrmann, A. Carbon Nanotube Network Ambipolar Field-effect Transistors with 108 on/off Ratio. *Adv. Mater.* **2014**, *26*, 5969−5975.
(61) Sarker, B. K.; Shekhar, S.; Khondaker, S. I. Semiconducting Enriched Carbon Nanotube Aligned Arrays of Tunable Density and Their Electrical Transport Properties. *ACS Nano* **2011**, *5*, 6297−6305.
(62) Yu, Z.; Burke, P. J. Aligned Array FETs as a Route toward THz Nanotube Transistors. *In Terahertz for Military and Security Applications III*; International Society for Optics and Photonics, 2005; *5790*, 246−254.
(63) Bindl, D. J.; Wu, M.-Y.; Prehn, F. C.; Arnold, M. S. Efficiently Harvesting Excitons from Electronic Type-Controlled Semiconducting Carbon Nanotube Films. *Nano Lett.* **2011**, *11*, 455−460.
(64) Brady, G. J.; Way, A. J.; Safron, N. S.; Evensen, H. T.; Gopalan, P.; Arnold, M. S. Quasi-Ballistic Carbon Nanotube Array Transistors with Current Density Exceeding Si and GaAs. *Sci. Adv.* **2016**, *2*, No. e1601240.
(65) Fadil, F.; Affandi, N. D. N.; Misnon, M. I. Identification of Surfactants Aggregates on Graphitic Surface of Carbon Nanotubes. *J. Exp. Nanosci.* **2019**, *14*, 23−32.


https://dx.doi.org/10.1021/acsomega.0c04607
*ACS Omega* 2021, 6, 5146−5157